

Title	Design and Control of JAIST Active Robotic Walker
Author(s)	Lee, Geunho; Ohnuma, Takanori; Chong, Nak Young
Citation	Journal of Intelligent Service Robotics, 3(3): 125-135
Issue Date	2010-07
Type	Journal Article
Text version	author
URL	<a href="http://hdl.handle.net/10119/9064">http://hdl.handle.net/10119/9064</a>
Rights	This is the author-created version of Springer, Geunho Lee, Takanori Ohnuma, and Nak Young Chong, Journal of Intelligent Service Robotics, 3(3), 2010, 125-135. The original publication is available at <a href="http://www.springerlink.com">www.springerlink.com</a> , <a href="http://dx.doi.org/10.1007/s11370-010-0064-5">http://dx.doi.org/10.1007/s11370-010-0064-5</a>
Description	

# Design and Control of JAIST Active Robotic Walker

Geunho Lee · Takanori Ohnuma · Nak Young Chong

Received: date / Accepted: date

**Abstract** This paper presents the design and control of a novel assistive robotic walker that we call “JAIST active robotic walker (JARoW)”. JARoW is developed to provide potential users with sufficient ambulatory capability in an efficient, cost-effective way. Specifically, our focus is placed on how to allow easier maneuverability by creating a natural interface between the user and JARoW. For the purpose, we develop a rotating infrared sensor to detect the user’s lower limb movement. The implementation details of the JARoW control algorithms based on the sensor measurements are explained, and the effectiveness of the proposed algorithms is verified through experiments. Our results confirmed that JARoW can autonomously adjust its motion direction and velocity according to the user’s walking behavior without requiring any additional user effort.

**Keywords** welfare robotics, active walker, natural interface, proximity sensor, easy maneuverability

## 1 Introduction

The elderly population is growing fast all over the world. Japan is the most rapidly aging country, and its population aged 65 or above rose to more than 21 percent of the whole population in 2008. Japan is projected to become a super-aged society where those aged 65 or above account for about 36 percent by 2050. Population aging will cause significant challenges of caregiving. Therefore, for instance, a personal assistive mobility device is strongly desired to keep the elderly independent.

---

G. Lee, T. Ohnuma, and N.Y. Chong  
School of Information Science,  
Japan Advanced Institute of Science and Technology (JAIST)  
1-1 Asahidai, Nomi, Ishikawa 923-1292, Japan  
E-mail: {geun-lee, t-ohnuma, nakyoung}@jaist.ac.jp



Fig. 1 JAIST active robotic walker (JARoW) prototype

Recent advances in robot technology have made it possible to design a wide variety of assistive devices [1]-[3]. Specifically, robotic walking aids have been developed for the elderly and/or lower limb disabled people. Notable examples include robotic wheelchair [4][5], robotic cane [6][7], powered exoskeleton [9]-[11], and robotic walker [12]-[18]. These mobility assistive devices provided users with a certain level of ambulatory capability toward independent living. However, there remains further progress to be made toward more widespread use of such devices. There are many points of consideration when developing a walking aid for the elderly. A major premise is that the elderly are slow in behavior and not familiar with mechanical or electronic controls. Moreover, they want to be able to continuously use their own device in daily routines. They need to go to an elevator or bathroom, and navigate in a narrow, crowded hallway.

The main purpose of this paper is to present our new development that we call “JAIST active robotic walker

(JARoW)” as shown in Fig. 1. The JARoW prototype is developed to provide potential users with sufficient ambulatory capability in all directions and easy-to-use features. What is the most important aspect from the practical point of view is to develop an active yet compact prototype not requiring any artificial controls. There is always a challenge on how to design a natural user interface. For the purpose, we employ a pair of rotating infrared sensors detecting the location of the user’s lower limbs. Based on the results obtained from preliminary experiments, two main control algorithms are proposed, enabling to control JARoW without any special-purpose artificial interface. The control algorithms estimate the location of the user’s lower limbs in real time, and allow the potential users to walk naturally. This paper details how to realize the walker control algorithms to facilitate the use of the proposed interface. We perform extensive experiments to demonstrate the effectiveness of both the interface and the control algorithms for the JARoW prototype in our laboratory environment.

The rest of this paper is organized as follows. Section 2 gives a brief description on the state-of-the-art of robotic walkers and their interfaces. Section 3 presents mechanical design, fabrication, and integration of the JARoW prototype. Section 4 introduces the preliminary test results for the interface system. Section 5 describes the main control algorithms that will induce the desired motion of JARoW. Section 6 illustrates experimental results and discusses our future directions. Section 7 draws our conclusions.

## 2 Background

For the elderly and/or lower limb disabled people, there have been many examples of prototype and robotic walking aids such as robotic wheelchair [4][5], robotic cane [6][7], robotic crutch [8], powered exoskeleton [9]-[11], and robotic walker [12]-[18]. Among them, wheelchairs [4][5] are the most widely used mobility aids. Unanticipated problems reported include muscle weakness due to long-time sitting or mental stress from the lower line-of-sight. Powered exoskeletons [9]-[11] supply the activation-energy for limb movement. However, the elderly most probably find it very uncomfortable to wear. It is also troublesome to wear and unwear repeatedly whenever needed. Robotic walkers can be further divided into passive [12]-[15] and active walkers [16]-[18]. The features of passive walkers include low cost, simple structure, and compact size, which enable them to be easily fit for use in our daily environment. However, it is deemed to be unsafe for the elderly to use the walker on uneven/slope terrain. On the other hand, the active

walkers provide both transportation aid for indoor and outdoor use and ambulatory rehabilitation. The problems with the active walkers are that they are still bulky and costly. Moreover, their complicated operation often requires considerable skill to use, and careless operation may cause an accident.

A simple and user-friendly interface is of particular importance. In detail, the user interface should be able to adapt to users with different levels of physical and mental functionality. Users should be easy to learn it and then be able to use it naturally. These interface can be broadly classified into direct and indirect types, according to whether the user’s command or intention is directly passed to the walking devices. Direct interfaces include joysticks [19]-[21], switches and buttons [22][23] (or touch screens [24]-[26]), and voice communications [27][28]. To offer more sophisticated interactions, studies using force sensing and control are presented in [14][19]. When the joystick is moved in any direction during walking, vibrations may appear due to the foot strike or uneven terrain. Toward simpler and easier controls, switches and buttons [22][23] or touch screens [24]-[26] have been developed and applied to the robotic walker or the robot guide. As compared with the joystick, due to their discrete or intermittent operation, mental workload might increase. Moreover, the interface may cause a confusion for elderly users, which might result in an accident. Recently the user interfaces using voice communication have been presented in [27][28]. The voice communication has an advantage of transferring effective high-level commands as a bilateral communication tool. However, there are critical problems such as interference and recognition to be resolved. At the opposite end, indirect user interfaces recognize the user’s motion and/or intention without requiring manual operations. Several examples include the visual recognition using cameras [29][30] and human gait detection based on pressure sensors [31][32]. However, we need to incorporate an elaborate recognition algorithm and high performance devices into the visual recognition system. Human gait detection also requires an additional device worn on the human body and its outdoor environments remains a difficult problem. To overcome those limitations of existing indirect interfaces, we attempt to develop a novel natural interface system in this work.

## 3 System Description

### 3.1 Mechanical Design

Our mechanical design concept is to assist the elderly to do their daily routines. Due to its compact size: 825

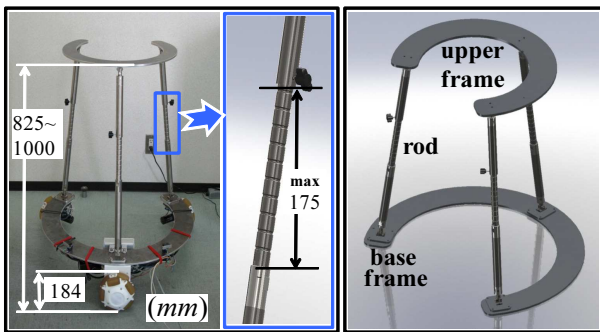


Fig. 2 Mechanical structure of JARoW

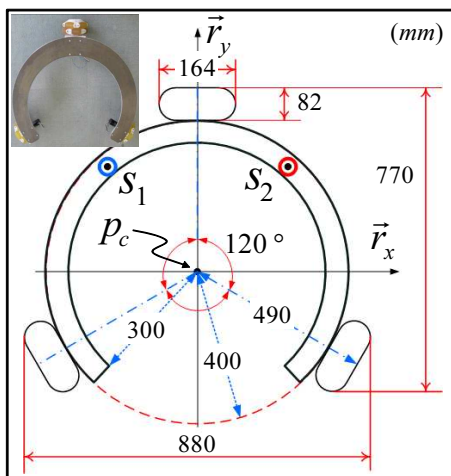


Fig. 3 Specification and notations of the base frame

$\sim 1000$  mm in height, and 880 mm and 770 mm in horizontal diameters, it is considered to be suited for use in various environments including narrow hallways or elevators. See Figs. 2 and 3. The outline is a circular shape to reduce possible collisions with obstacles or walls. Its light weight of 20 kg is achieved by the use of an aluminum alloy.

As shown in Fig. 2, JARoW has three main structural parts: base frame, upper frame, and connecting rods. The base frame is to support the superstructure and is directly connected to three omni-directional wheels. The base frame is equipped with proximity sensors detecting the user's lower limb location. The length of the connecting rod can be changed up to 175 mm according to the height of potential users. The users are able to lean their upper body forward and place their forearm onto the upper frame. As illustrate in Fig. 3, the JARoW prototype has its local coordinates  $\vec{r}_x$  and  $\vec{r}_y$ . Here,  $\vec{r}_y$  defines the vertical axis as its heading direction, and  $\vec{r}_x$  denotes the horizontal axis by rotating  $\vec{r}_y$  90 degrees counterclockwise. The center position is denoted as  $p_c$ . Finally,  $S_1$  and  $S_2$  denote the positions of a pair of proximity sensors.

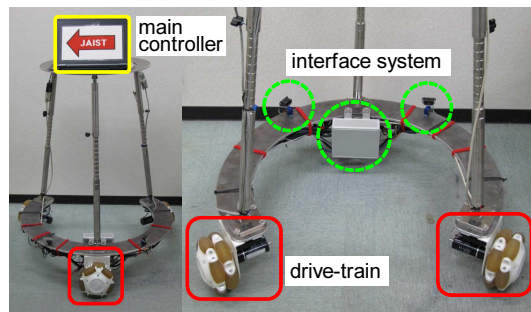


Fig. 4 Three components in wheel drive system

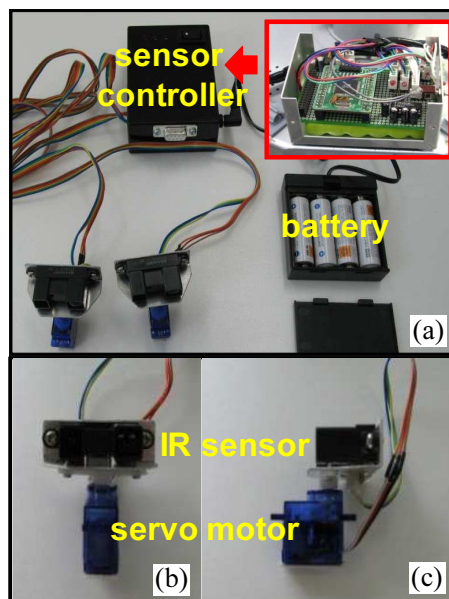


Fig. 5 User interface system: (a) sensor module components, (b) front view of sensor module, (c) side view of sensor module

### 3.2 Wheel Drive System

The wheel drive system includes the drive-train, the interface system, and the main controller as shown in Fig. 4. We use a laptop PC that runs on Microsoft's Windows XP as the main controller on top of the upper frame. Further details of the main controller's functions will be explained in Section 5.

The drive-train is composed of three omni-directional wheels, three motors fully equipped with encoder and a 34:1 gear reduction unit, three motor drivers, and the motor controller. Three omni-directional wheels are mounted underneath the base frame 120 degrees apart from each other, allowing the walker to move forward and backward, slide sideways, and rotate at the same spot. Such omni-directionality provides a very efficient means of direction control in highly cluttered environments. The maximum stall torque is determined in such a way that JARoW accommodates up to 90 kg. It is reported that the average maximum walking speed for

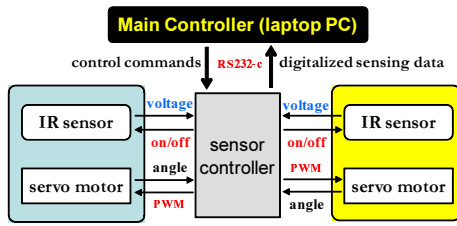


Fig. 6 Diagram for the control architecture of IR sensor

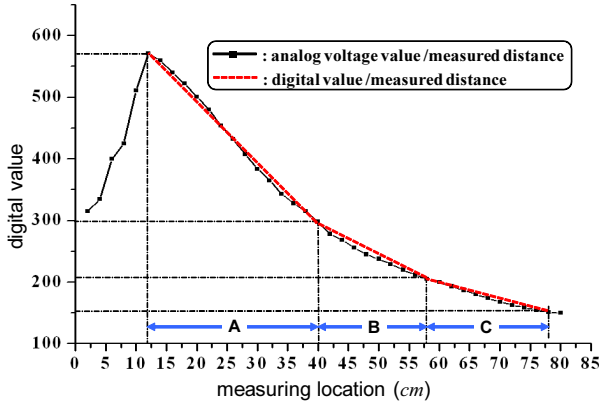


Fig. 7 Input-output relationship of the 10-bit A/D converter

elderly pedestrians is  $4.8 \text{ km/h}$  on flat terrain [33]. The maximum continuous torque is determined to meet the maximum velocity requirement,  $6.58 \text{ km/h}$ , of the drive-train. Thus, the prototype is believed to be capable of supporting the elderly with trouble walking and those with weakened leg muscles.

In practice, we detect the location of the user's lower limbs inside the base frame using the infrared sensors rotating about their vertical axis. As presented in Fig. 5, the interface system is composed of a pair of infrared sensor modules and their controller. Each sensor module has the MiniStudio MiniS RB90 servo motor and the Sharp GP2Y0A21 infrared sensor, mounted on top of the base frame (see Fig. 4). The Atmel ATmega128 microcontroller controls each servo motor rotating the infrared sensor and feeds the measured data to the main controller. Fig. 6 indicates the diagram for the control architecture of the interface system. The sensor controller forwards the control signal to each sensor module, which controls the rotation angle and speed of the servo motor by pulse width modulation. In addition, the analog output voltage representing the sensor-to-surface distance is fed to the controller and converted to 10-bit digital values. In Fig. 7, the black solid line and the red dashed line indicate the analog output voltage and the converted digital value, respectively. The infrared sensors can measure a distance range from  $12 \text{ cm}$  to  $180 \text{ cm}$ . Inside the base frame, we only use a range of  $12 - 70 \text{ cm}$ . Based on the analog-digital dis-

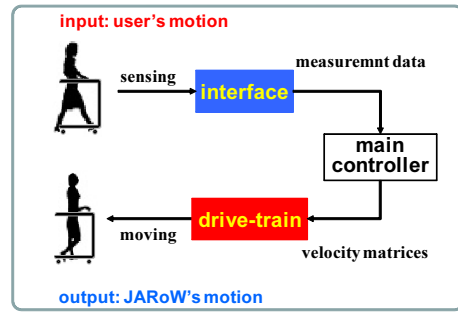


Fig. 8 Schematic for the overall control flow

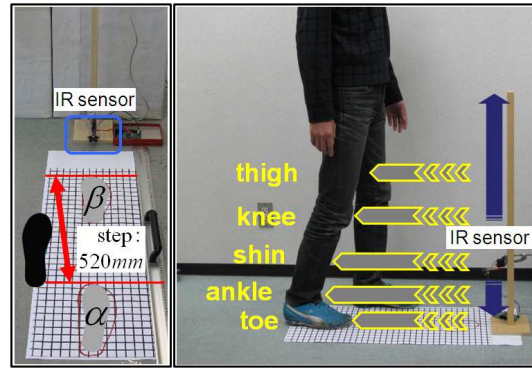


Fig. 9 Preliminary lower limb measurement test

tance relation, the effective range is divided into three sections, and the linearized digital values represented by the red dashed lines in Fig. 7 are used to measure the surfaces of lower limbs.

### 3.3 Control Architecture

Fig. 8 shows the overall control flow schematic. The input to the main controller includes the lower limb position data obtained from the interface system. Based on the data, the observation algorithm estimates the current location of the lower limbs with respect to the walker's local coordinate system. Then, the motion control algorithm outputs the desired velocity matrix for each motor at each time step. Details of these algorithms will be explained in Section 5.

## 4 Preliminary Analysis of Interface System

In this section, we present and summarize the preliminary test results for the proposed interface system. The interface allows the user to control JARoW without any effort using the main control algorithms.

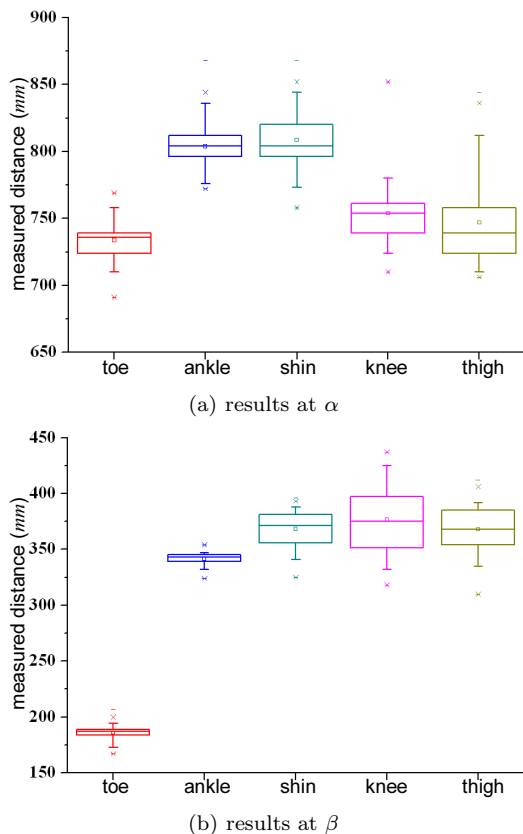


**Fig. 10** Shin measurement results at  $\alpha$  and  $\beta$  performed in Fig. 9

#### 4.1 How to detect the lower limb movement?

JARoW is designed to provide potential users with simple yet effective control of moving it forward, backward, and turning even in crowded and compact areas. We estimate the user's lower limb states using the infrared sensors. It enables automatic control of the JARoW velocity, without employing electronic devices worn on the user body or manual controls such as joysticks or touchpads. We attempt to replace the burden of sophisticated hardware, software, and heaps of hard-to-remember safety and operating rules with the proposed user interface. JARoW moves to a desired position and direction, corresponding to the user's lower limb position relative to its base frame. Now the question is where and how to measure the position of the user's lower limb?

Fig. 9 shows the test scene, where we measured the distance of two consecutive right footsteps at the pre-determined positions  $\alpha$  and  $\beta$ . The right leg moved forward 100, 260, and 520 mm, respectively. We collected 300 sets of measurements. The results for the 520 mm interval are presented in Fig. 10 and Table 1. In Fig. 10, the error bars represent the 95% confidence intervals

**Table 1** Comparison of data measured at  $\alpha$  and  $\beta$  (mm)

	$\alpha$			$\beta$			$\alpha - \beta$
	mean	max.	min.	mean	max.	min.	mean
toe	733.7	691	769	186.1	167	207	547.6
ankle	803.9	772	868	341.7	324	354	462.1
shin	808.7	758	868	368.2	325	396	440.5
knee	753.8	710	852	376.3	318	437	377.5
thigh	746.8	706	844	367.8	310	412	378.9

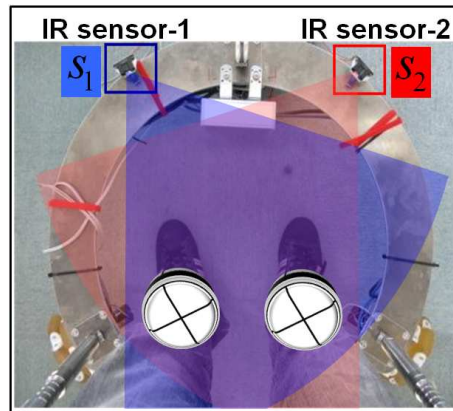


**Fig. 11** Lower leg modeled as a cylinder with a radius  $d$

and the boxes indicate distributions of measured data in the range of 25% to 75%. Table 1 shows the mean values, minimum values, and maximum values at  $\alpha$  and  $\beta$ . Moreover,  $\alpha - \beta$  indicates the mean of measured interval distance. Similar results were also observed in other intervals.

From the results in Fig. 10, the toe interval is the closest to the actual footstep interval. The higher measuring location in the leg, the worse results we obtained. This is due to possible changes in knee angle. However, the proximity sensors are difficult to be mounted at the same level as the toes. Some potential difficulties and problems include: 1) toes may disappear from the sensing area due to elevation changes, and 2) the proximity sensors may collide with the terrain. As a second best option, we determine to measure the shin location, since the shin data showed a uniform distribution and a near-constant value. The lower leg can be modeled as a cylinder with a radius  $d$  as shown in Fig. 11. As a pair of infrared sensors rotate a certain angle horizontally, the shin location measurement can accommodate individuated lower leg movements.

We compared the accuracy of the shin distance measurement between the infrared sensor and one of the most widely used laser sensors (Hokuyo Ltd.'s URG-04LX). Fig. 12 illustrates the result of 300 trials where the error bars represent the 95% confidence intervals and the boxes indicate distributions of measured data

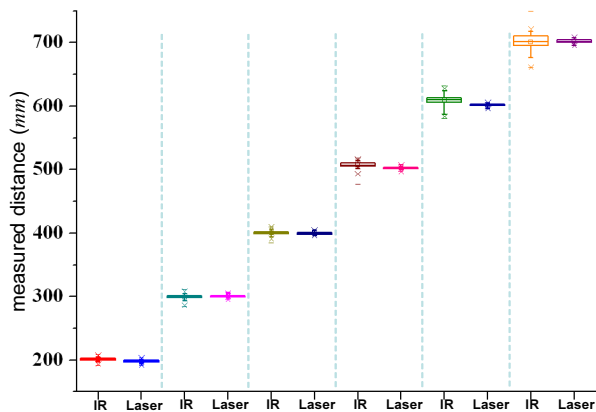


**Fig. 12** Distance measurement of the right shin using the infrared and laser sensors

in the range of 25% to 75%. As can be seen from the figure, the laser sensor outperformed the infrared sensor in terms of accuracy, but the infrared sensor also showed reasonably good accuracy.

#### 4.2 How to estimate the walking state?

Now we estimate the walking state using the shin distance measurements. As illustrated in Fig. 13, for instance, the forward, backward, and halt state are identified from the raw infrared sensor measurements. The area within the base frame is represented as a rectangle with  $600 \times 700$  mm, and is further divided into six rectangular grids. Each grid is numbered from the upper left to lower right. We empirically saw five shin location patterns. If the shins are detected at #III and #IV, it is considered as the halt state. It is assumed that the left lower leg and the right lower leg are located at the oddly and the evenly numbered grids, respectively. If one shin is detected at #III or #IV and the other is detected at #I or #II, it is considered as the forward state. Likewise, when either of the lower legs is located at #V or #VI, it is considered as the backward state. For the halt state, the main controller outputs the velocity matrix with all zero elements. When either the forward or backward state is identified, the elements of the velocity matrix have a certain set of values.

### 5 Main Control Algorithms

#### 5.1 Observation Algorithm

The key to the observation algorithm lies in obtaining reliable measurements of the shin locations. The observation algorithm is implemented through the following three steps. First, the measurement step constructs two

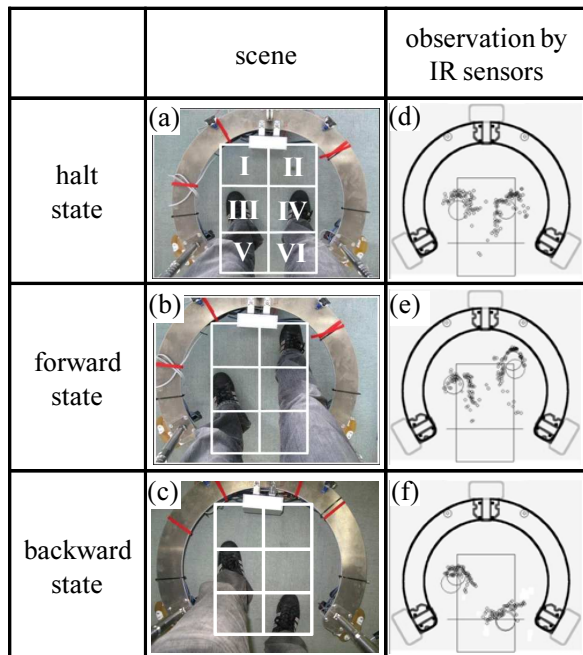


**Fig. 13** Preliminary test for mobility state identification

one-dimensional arrays in a memory of the main controller as illustrated in Fig. 14-(a). As each sensor  $S_i$  scans  $\pm 30$  degrees at regular intervals in Fig. 14-(b), the distance to the shin is recorded in the corresponding cell of the first array. At the same time, the servo motor angle is recorded in the second array so that the distance array corresponds to the motor angle array. Then, the controller checks their distance array cells that contain a non-zero value (from the lower bound  $d_{min}$  to the upper bound  $d_{max}$ ) and reads the corresponding angle array cells.

Secondly, the extraction step extracts reliable data from the output of the measurement step, and transforms it into the JARoW coordinate format. For the purpose, a  $30 \times 30$  2-D grid with  $3$  cm  $\times$   $3$  cm unit cells is built. Using the distance and angle array data, the position estimates are stored in the corresponding cell as an integer intensity value. Once a full 60 degree scanning is completed, as illustrated in Fig. 14-(c), the Sobel edge detection algorithm [34] improves the original surface detection data.

Thirdly, the calculation step is to calculate the shin locations. After collecting the cells with the non-zero value from  $d_{min}$  to  $d_{max}$  based on the output of the extraction step, the three feature points,  $p_{min}$ ,  $p_{max}$ , and  $p_s$  are specified using  $d_{min}$ ,  $d_{max}$ ,  $c_{dis}$  and their corresponding cells in the angle array, respectively. For  $p_s$ , by computing the average of a sequence of numeric values in the angle array, the cell containing the value equal or closest to the average is selected, and the center angle

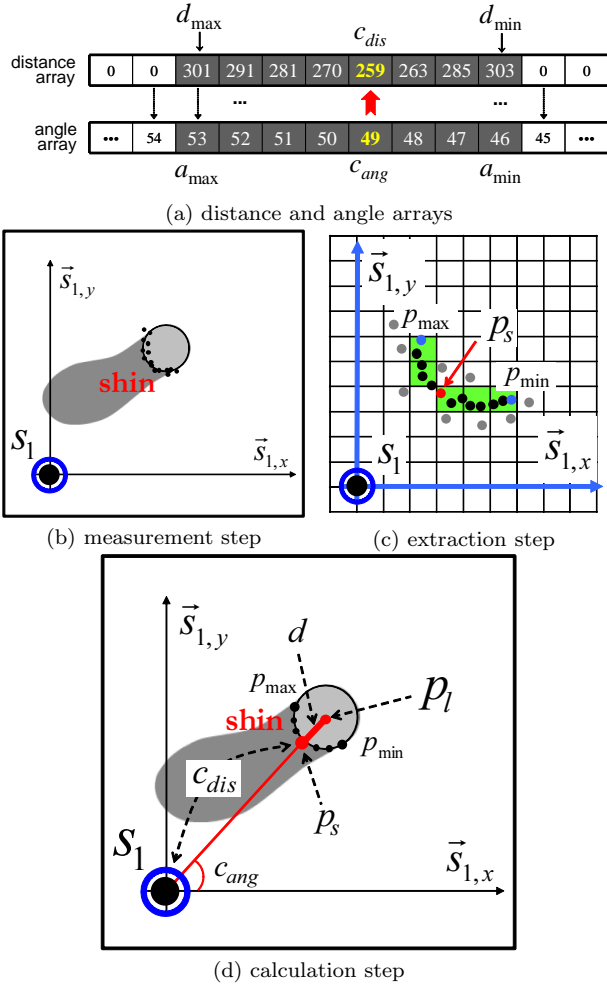


Fig. 14 Illustration of the observation function

$c_{ang}$  to this value is set. The distance cell corresponding  $c_{ang}$  is defined as the center distance  $c_{dis}$ . Thus,  $p_s$  is computed based on  $c_{dis}$  with the minimum distance value among the cells and  $c_{ang}$ . To identify the shin shape, the following two conditions should be further satisfied. The first condition checks whether the radius of curvature is reasonably similar to the shin shape. The second condition tests whether the two line segments  $\overline{p_{min}p_s}$  and  $\overline{p_{max}p_s}$  are symmetric with respect to the JARoW's vertical axis, and the angle between them falls within a certain range. Through the above process, if the shin is recognized, its center point  $p_l$  can be obtained by adding  $c_{dis}$  to the radius  $d$  (see Fig. 14-(d)). Consequently, at time  $t$ , the observation algorithm outputs the left and right lower leg locations,  $p_{l,t}$  and  $p_{r,t}$ .

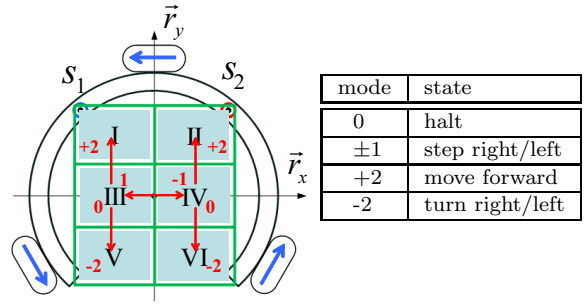


Fig. 15 JARoW motion control state

## 5.2 Motion Control Algorithm

There are four types of walking states, each of which corresponds to a particular lower leg placement as shown in Fig. 15. For safety reasons, backward motion is replaced by combining turning back and forward motion. Here  $g_{l,t}$  and  $g_{r,t}$  denote the grids occupied by the left and right legs, respectively, at time  $t$ . Similarly,  $g_{l,t-1}$  and  $g_{r,t-1}$  denote the grids occupied by the left and right legs, respectively, at time  $t-1$ . Now the walking state at  $t$  is determined by subtracting  $g_{l,t}$  (or  $g_{r,t}$ ) from  $g_{l,t-1}$  (or  $g_{r,t-1}$ ). For example, if  $p_{l,t-1}$  and  $p_{r,t-1}$  belong to #III and #IV, and  $p_{l,t}$  and  $p_{r,t}$  belong to #III and #VI, respectively, the walking state is -2, and the walker begins its turning motion to the right. The travel distance  $d_r$  or the rotation angle  $\theta_r$  is computed as follows. First,  $d_r$  is given by

$$d_r = d_f/2, \quad (1)$$

where  $d_f$  indicates the stride length of either the left or the right foot. Empirically, the denominator in (1) is selected such that the upper body (or the walker) moves one-half the stride length. Secondly, let us say that we have a triangle at  $t$  formed by connecting the three points  $p_{c,t}$ ,  $p_{r,t}$ , and  $p_{r,t-1}$  in Fig. 16, where  $p_{c,t}$  indicates the centroid of the walker at  $t$ , and  $p_{r,t}$  and  $p_{r,t-1}$  are the right leg positions at  $t$  and  $t-1$ , respectively.  $d_t$ ,  $d_f$ , and  $d_{t-1}$  denote the side lengths of  $\triangle p_{c,t}p_{r,t}p_{r,t-1}$ , respectively. Using Heron's formula [35] in geometry, the area  $A_r$  of  $\triangle p_{c,t}p_{r,t}p_{r,t-1}$  can be calculated by:

$$A_r = \sqrt{s(s-d_t)(s-d_{t-1})(s-d_f)}, \quad (2)$$

where  $s$  is the semiperimeter of  $\triangle p_{c,t}p_{r,t}p_{r,t-1}$  given by  $(d_t + d_{t-1} + d_f)/2$ .  $d_x$  denotes the distance from  $p_{c,t}$  to an intersection point  $p_i$  between  $\vec{r}_x$  and  $\overline{p_{r,t}p_{r,t-1}}$ . Using the sine formula,  $A_r$  is computed:

$$A_r = \frac{1}{2}d_x d_f \sin \theta_r. \quad (3)$$

Now  $\theta_r$  is obtained:

$$\theta_r = \sin^{-1}\left(\frac{2A_r}{d_x d_f}\right). \quad (4)$$

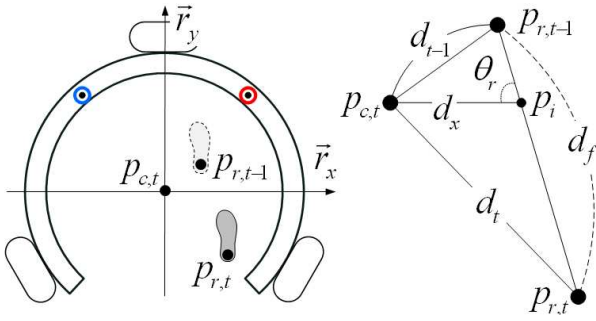


Fig. 16 Computation of the turning angle  $\theta_r$

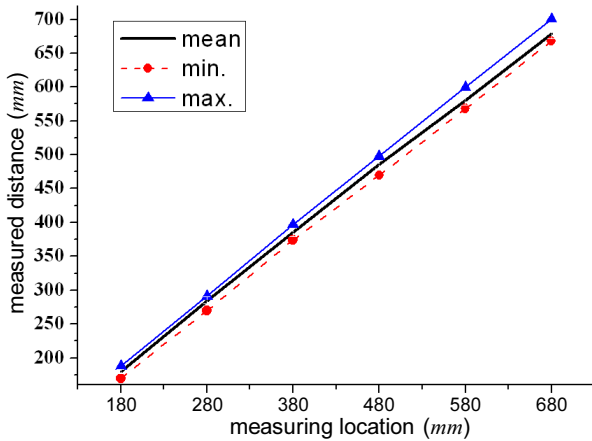


Fig. 17 The shin distance measurements by the observation algorithm

Based on  $p_{l,t}$  and  $p_{r,t}$  of the observation algorithm, the main controller identifies the grids that correspond to the shin locations. Next, the control mode is calculated with  $d_r$  or  $\theta_r$  using (1) and (4). Diving  $d_r$  and  $\theta_r$  by the sensor measurement time interval, the controller obtains the desired walker velocities  $\dot{x}$ ,  $\dot{y}$ , and  $\dot{\theta}_r$ . The rotational velocities of the individual wheels,  $\omega_0$ ,  $\omega_1$ , and  $\omega_2$ , are obtained as follows:

$$\begin{bmatrix} \omega_0 \\ \omega_1 \\ \omega_2 \end{bmatrix} = \frac{1}{r} \begin{bmatrix} -1 & 0 & 0.4 \\ \frac{1}{2} & -\frac{\sqrt{3}}{2} & 0.4 \\ \frac{1}{2} & \frac{\sqrt{3}}{2} & 0.4 \end{bmatrix} \begin{bmatrix} \dot{x} \\ \dot{y} \\ \dot{\theta}_r \end{bmatrix}, \quad (5)$$

where  $r$  denotes the wheel radius.

## 6 Experimental Results and Discussion

This section presents our experiment results of the running test of the walker. The walker moves with the maximum velocity of 4.8 km/h. To verify the effectiveness of the observation algorithm, we measured the distance to the shin placed at six different locations. The radius  $d$  of the lower leg is set to 50 mm. Two infrared proximity sensors emit an infrared ray every one degree while

Table 2 Statistical analysis of measurement data of Fig. 17 (mm)

real	180	280	380	480	580	680
mean	180.02	284.95	385.65	485.38	580.54	678.93
sd	3.32	5.12	5.97	6.15	6.96	7.34
min	170	270	374	470	568	668
max	188	291	397	498	600	704
range	18	21	23	28	32	36

rotating 60 degrees with 308 deg/s. We obtained reasonably precise estimates of the lower leg center positions. Fig. 17 and Table 2 show the statistical analysis results over 300 measurements. In Fig. 17, the black bold solid line, red dotted line, and blue solid line indicate the mean value, minimum value, and maximum value, respectively. Compared with Fig. 12, Fig. 17 and Table 2 show enhanced measurement accuracy.

To examine the walker movement accuracy responding to the user's motion, the forward motion test was performed. In this test, as a subject takes steps of uniform length of 300 mm forward, the walker follows the stride length as closely as possible. Fig. 18-(a) shows the result for 233 steps. The mean value, the standard deviation, the minimum value, and the maximum value are 302.6 mm, 26.2, 224 mm, and 394 cm, respectively. We enlarge a specific range from the 101st step to the 130th step in Fig. 18-(b) and -(c). The results show that the walker can generate the forward motion corresponding to actual user stride lengths and stride rates. It is also confirmed that the control approach based on the shin distance measurement is robust against transient faults such as the measurement error in previous time steps.

Next, to investigate the validity of the proposed motion control algorithm, as shown in Fig. 19-(a), the circular path following experiment was performed. Here, a subject walks along the circular path with the radius of 1 m clockwise and counterclockwise. Fig. 19-(b) shows the resulting walker motion, where the square and circular dots indicate the walker center points, and the straight lines between the dots are actual trajectories. This experiment demonstrated that the walker could adjust its motion according to the user's walking speed and direction under the proposed motion control algorithm.

Finally, we performed a long distance test in an indoor environment. Fig. 20 shows snapshots for the forward movements in a hallway. In Fig. 21, it moves forward and goes around a corner. It is observed that the walker is controlled successfully in the indoor environment requiring a turning motion. Moreover, as shown in Fig. 22, the walker turns on the spot in an elevator.

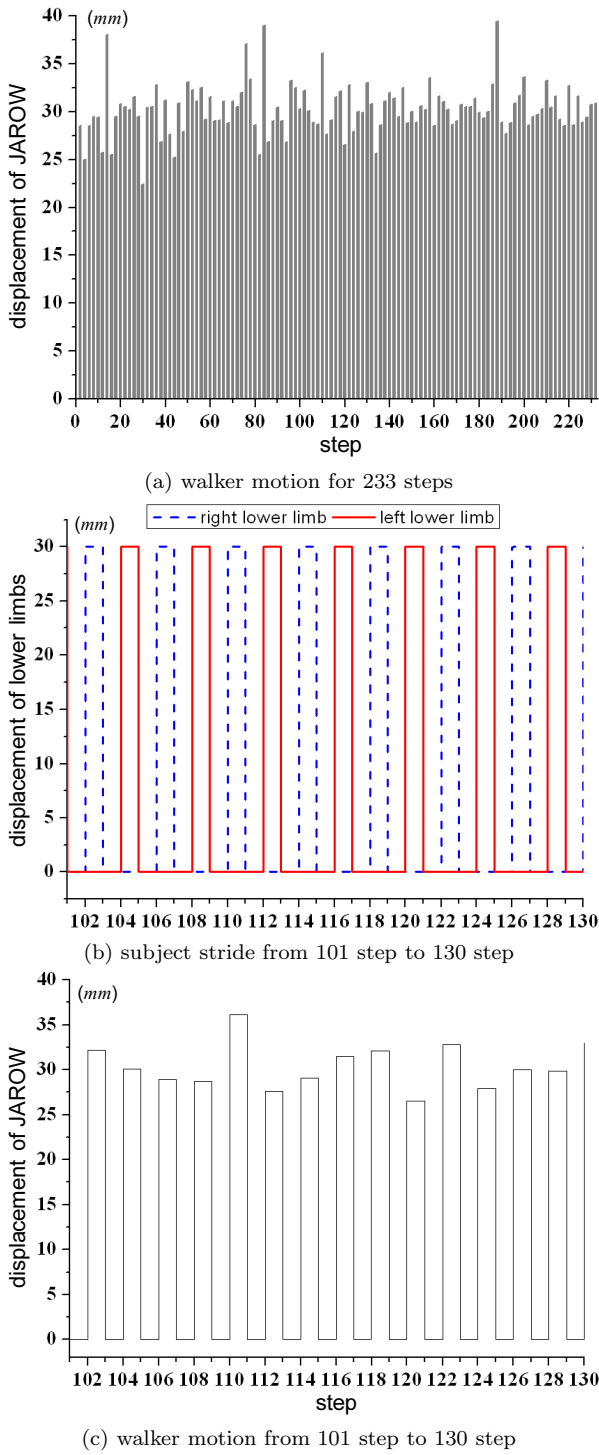


**Fig. 18** JARoW displacement according to the regular stride lengths

The results verify that the walker works satisfactorily under our experimental conditions. In contrast to existing active-type walkers, our walker features simple structure and compact size that can be fit into our everyday environment. More notably, the proposed user

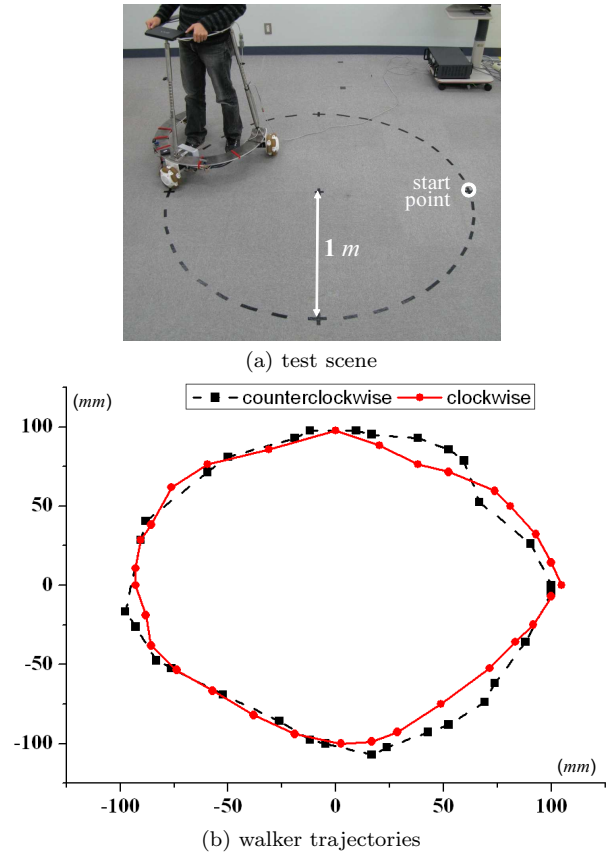


**Fig. 19** Experimental result for following a circular trajectory

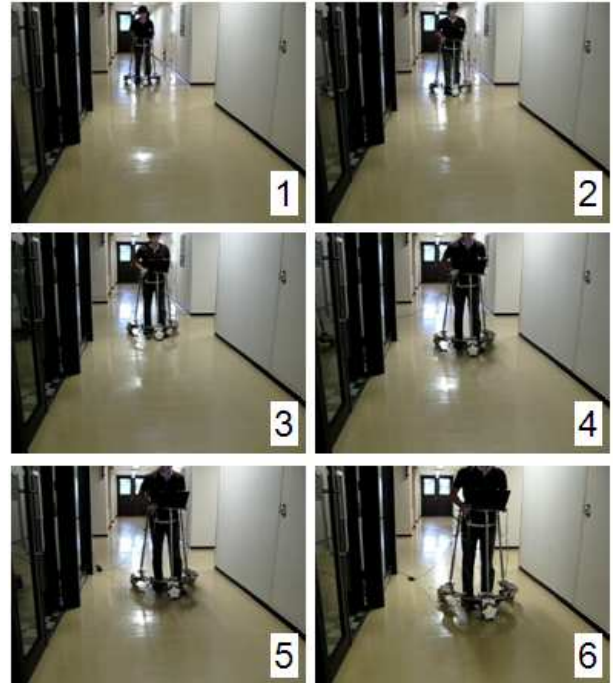


**Fig. 20** Forward movement of the JARoW in a hallway

interface system allows the user to easily control the walker without requiring any mental or physical efforts.

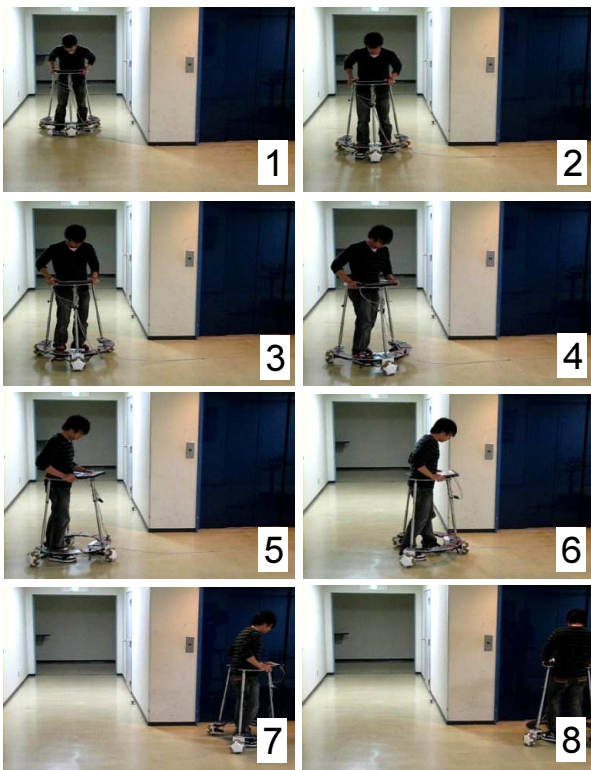


**Fig. 21** Forward and rotational movement of the JARoW in a hallway with a corner

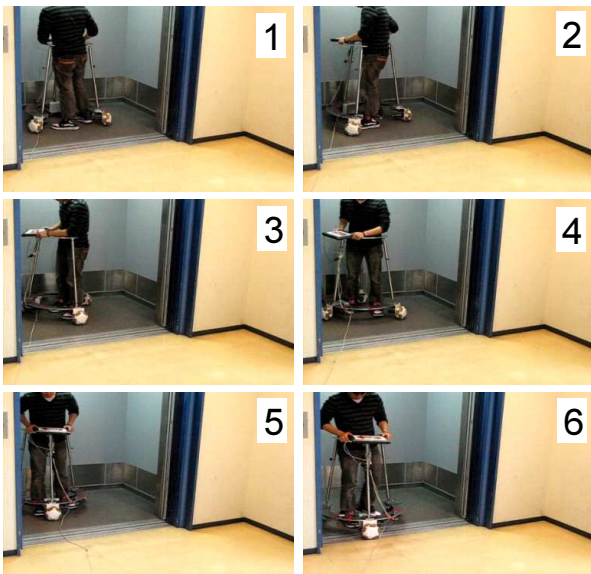


**Fig. 22** Rotation movement of the JARoW in an elevator

There still remain several issues to be resolved. First of all, the walker must be able to provide a natural and smooth movement. As mentioned earlier, the walker updates the observation results after the sensors rotate 60 degrees. It may cause the walker to move rather intermittently. Also, the human gait control system is non-linear, and the gait parameters vary across users. We

are currently developing a particle filter-based lower leg position estimation and prediction system to recognize the user's walking intention from noisy sensor signals. When considering the elderly who tend to lean their upper body onto the walker, a more sophisticated controller will be needed to cope with dynamic and unpredictable changes in the nominal walker parameters. A reliable and cost-effective control solution will be incorporated into the next prototype.

## 7 Conclusions

This paper presented the first version of our robotic walker enabling the frail elderly to enjoy an independent lifestyle. We designed, manufactured, and controlled the active yet compact prototype. In particular, we proposed a novel interface system without requiring any user operations, which senses the location of the user's lower limbs through the use of rotating infrared sensors. We also developed the control algorithms to adjust the motion of the walker according to the user's walking speed and direction. Various experiments were demonstrated in our laboratory environments to show the effectiveness of the prototype. The results so far are encouraging, and more sophisticated algorithms are to be designed to further improve the walker maneuverability and control.

## References

1. M. Topping, "An overview of development of Handy-1, a rehabilitation robot to assist the severely disabled," *Artificial Life and Robotics*, vol.4, no.4, pp.188-192, 2000.
2. R. Soyama, S. Ishii, and A. Fukase, "The development of meal-assistance robot 'My Spoon'," *Proc. 8th IEEE Int. Conf. Rehabilitation Robotics*, pp.88-91, 2003.
3. G. R. B. E. Romer, H. J. A. Stuyt, G. Peters, and K. V. Woerden, "The current and future processes for obtaining a 'Manus' (ARM) rehabrobot within the Netherlands," *Proc. 8th IEEE Int. Conf. Rehabilitation Robotics*, pp.9-12, 2003.
4. H. Ikeda, Y. Katsumata, M. Shoji, T. Takahashi, and E. Nakano, "Cooperative strategy for a wheelchair and a robot to climb and descend a step," *Advanced Robotics*, vol.22, no.13-14, pp.1439-1460, 2008.
5. C.-H. Kuo, H.-W. Yeh, and C.-E. Wu, "Development of autonomous navigation robotic wheelchairs using programmable system-on-chip based distributed computing architecture," *Proc. IEEE Int. Conf. Systems, Man and Cybernetics*, pp.2939-2944, 2007.
6. I. Shim, J. Yoon, and M. Yoh, "A Human Robot Interactive System 'RoJi'," *International Journal of Control, Automation, and Systems*, vol.2, no.3, pp.398-405, 2004.
7. H. Yu, M. Spenko, and S. Dubowsky, "An adaptive shared control system for an intelligent mobility aid for the elderly," *Autonomous Robotics*, vol.15, no.1, pp.53-66, 2003.
8. Y. Mori, J. Okada, and K. Takayama, "Development of a standing style transfer system 'able' for disabled lower

- limbs," IEEE/ASME Transactions on Mechatronics, vol.11, no.4, pp.372-380, 2006.
9. C. R. Kinnaird and D. P. Ferris, "Medial gastrocnemius myoelectric control of a robotic ankle exoskeleton," IEEE Transactions on Neural Systems and Rehabilitation Engineering, vol.17, no.1, pp.31-37, 2009.
  10. K. Suzuki, G. Mito, H. Kawamoto, Y. Hasegawa, and Y. Sankai, "Intention-based walking support for paraplegia patients with robot suit HAL," Advanced Robotics, vol.21, no.12, pp.1441-1469, 2007.
  11. A. B. Zoss, H. Kazerooni, and A. Chu, "Biomechanical design of the Berkeley lower extremity exoskeleton (BLEEX)," IEEE/ASME Transactions on Mechatronics, vol.11, no.2, pp.128-138, 2006.
  12. Y. Hirata, A. Hara, and K. Kosuge, "Motion control of passive intelligent walker using servo brakes," IEEE Transactions on Robotics, vol.23, no.5, pp.981-990, 2007.
  13. A. Veg and D. B. Popovic, "Walkaround: mobile balance support for therapy of walking," IEEE Transactions on Neural Systems and Rehabilitation Engineering, vol.16, no.3, pp.264-269, 2008.
  14. V. Kulyukin, A. Kutiyawala, E. LoPresti, J. Matthews, and R. Simpson, "iWalker: toward a rollator-mounted wayfinding system for the elderly," Proc. IEEE Int. Conf. RFID, pp.303-311, 2008.
  15. G. J. Lacey and D. Rodriguez-Losada, "The evolution of guido," IEEE Robotics and Automation Magazine, vol.15, no.4, pp.75-83, 2008.
  16. K. Kong and D. Jeon, "Design and control of an exoskeleton for the elderly and patients," IEEE/ASME Transactions on Mechatronics, vol.11, no.4, pp.428-432, 2006.
  17. H. Kobayashi, T. Karato, and T. Tsuji, "Development of an active walker as a new orthosis," Proc. IEEE Int. Conf. Mechatronics and Automation, pp.186-191, 2007.
  18. M. Tani, R. Suzuki, S. Furuya, and N. Kobayashi, "Internal model control for assisting unit of wheeled walking frames," Proc. IEEE Int. Conf. Control Applications, pp.928-933, 2004.
  19. A. J. Rentschler, R. Simpson, R. A. Cooper, M. L. Boninger, "Clinical evaluation of Guido robotic walker," Journal of Rehabilitation Research and Development, vol.45, no.9, pp.1281-1294, 2008.
  20. H. Hashimoto, A. Sasaki, Y. Ohyama, and C. Ishii, "Walker with hand haptic interface for spatial recognition," Proc. 9th IEEE Int. Work. Advanced Motion Control, pp.311-316, 2006.
  21. A. Morris, R. Donamukkala, A. Kapuria, A. Steinfield, J. Matthews, J. Dunbar-Jacobs, and S. Thrun, "A robotic walker that provides guidance," Proc. IEEE Int. Conf. Robotics and Automation, pp.25-30, 2003.
  22. G. Lacey and S. MacNamara, "User involvement in the design and evaluation of a smart mobility aid," Journal of Rehabilitation Research and Development, vol.37, no.6, pp.709-723, 2000.
  23. A. J. Rentschler, R. A. Cooper, B. Blasch, M. L. Boninger, "Intelligent walkers for the elderly: Performance and safety testing of VA-PAMAID robotic walker," Journal of Rehabilitation Research and Development, vol.40, no.5, pp.423-432, 2003.
  24. B. Graf, "An adaptive guidance system for robotic walking aids," Journal of Computing and Information Technology, vol.17, no.1, pp.109-120, 2009.
  25. H.-M. Shim, E.-H. Lee, J.-H. Shim, S.-M. Lee, and S.-H. Hong, "Implementation of an intelligent walking assistant robot for the elderly in outdoor environment," Proc. 9th IEEE Int. Conf. Rehabilitation Robotics, pp.452-455, 2005.
  26. B. Graf, M. Hans, and R. D. Schraft, "Care-O-bot II - development of a next generation robotic home assistant," Autonomous Robots, vol.16, no.2, pp.193-205, 2004.
  27. V. Kulyukin, "Human-robot interaction through gesture-free spoken dialogue," Autonomous Robots, vol.16, no.3, pp.239-257, 2004.
  28. S. MacNamara and G. Lacey, "A smart walker for the frail visually impaired," Proc. IEEE Int. Conf. Robotics and Automation, pp.1354-1359, 2000.
  29. H. Yano, Y. Hosomi, K. Aoki, R. Nanba, T. Hirotsu, and Satoru Okamoto, "Unstable motion detect system for four-casterd walker," IEICE technical report, Speech, vol.107, no.434, pp.13-18, 2008. (in Japanese)
  30. R. V. Rodriguez, R. P. Lewis, J. S. D. Mason, and N. W. D. Evans, "Footstep recognition for a smart home environment," International Journal of Smart Home, vol.2, no.2, pp.95-110, 2008.
  31. M. Hirasawa, H. Okada, and M. Shimojo "The development of the plantar pressure sensor shoes for gait analysis," Journal of Robotics and Mechatronics, vol.20, no.3 pp.324-330, 2007.
  32. K. Kong and M. Tomizuka, "Smooth and continuous human gait phase detection based on foot pressure patterns," Proc. IEEE Int. Conf. Robotics and Automation, pp.3678-3683, 2008.
  33. J. M. Burnfield and C. M. Powers, "Normal and pathologic gait" in *Orthopaedic Physical Therapy Secrets*, J. D. Placzek and D. A. Boyce (edt.), Hanley and Belfus (2nd ed.), 2006.
  34. R. C. Gonzalez and R. E. Woods, *Digital image processing*, 2nd ed. Prentice Hall, 2002.
  35. J. Vince, *Geometry for Computer Graphics: Formulae, Examples and Proofs*, Springer, 2004.